


RESEARCH ARTICLE

Open Access



An LQT2-related mutation in the voltage-sensing domain is involved in switching the gating polarity of hERG

Zhipei Liu^{2,3†}, Feng Wang^{1,2†}, Hui Yuan^{1,2†}, Fuyun Tian^{2,3†}, Chuanyan Yang^{2,3,4}, Fei Hu^{2,3}, Yiyao Liu², Meiqin Tang^{2,5}, Meixuan Ping^{2,3,6}, Chunlan Kang^{2,5}, Ting Luo^{2,7}, Guimei Yang^{1,2}, Mei Hu^{2,8}, Zhaobing Gao^{1,2,3,6*} and Ping Li^{1,2,3,6*} 

Abstract

Background Cyclic Nucleotide-Binding Domain (CNBD)-family channels display distinct voltage-sensing properties despite sharing sequence and structural similarity. For example, the *human Ether-a-go-go Related Gene* (hERG) channel and the Hyperpolarization-activated Cyclic Nucleotide-gated (HCN) channel share high amino acid sequence similarity and identical domain structures. hERG conducts outward current and is activated by positive membrane potentials (depolarization), whereas HCN conducts inward current and is activated by negative membrane potentials (hyperpolarization). The structural basis for the “opposite” voltage-sensing properties of hERG and HCN remains unknown.

Results We found the voltage-sensing domain (VSD) involves in modulating the gating polarity of hERG. We identified that a long-QT syndrome type 2-related mutation within the VSD, K525N, mediated an inwardly rectifying non-deactivating current, perturbing the channel closure, but sparing the open state and inactivated state. K525N rescued the current of a non-functional mutation in the pore helix region (F627Y) of hERG. K525N&F627Y switched hERG into a hyperpolarization-activated channel. The reactivated inward current induced by hyperpolarization mediated by K525N&F627Y can be inhibited by E-4031 and dofetilide quite well. Moreover, we report an extracellular interaction between the S1 helix and the S5-P region is crucial for modulating the gating polarity. The alanine substitution of several residues in this region (F431A, C566A, I607A, and Y611A) impaired the inward current of K525N&F627Y.

Conclusions Our data provide evidence that a potential cooperation mechanism in the extracellular vestibule of the VSD and the PD would determine the gating polarity in hERG.

Keywords hERG, K525N, Gating Polarity, Voltage-Sensing Domain, LQT2

[†]Zhipei Liu, Feng Wang, Hui Yuan, and Fuyun Tian contributed equally to this work.

*Correspondence:

Zhaobing Gao
zbgao@simm.ac.cn
Ping Li
lipingt@simm.ac.cn

¹ School of Pharmacy, Zunyi Medical University, Zunyi 563000, China

² Zhongshan Institute for Drug Discovery, Zhongshan 528400, China

³ Center for Neurological and Psychiatric Research and Drug Discovery, Shanghai Institute of Materia Medica, Chinese Academy of Sciences, Shanghai 201203, China

⁴ School of Basic Medicine and Clinical Pharmacy, China Pharmaceutical University, Nanjing 210009, China

⁵ School of Pharmaceutical Sciences, Southern Medical University, Guangzhou 510515, China

⁶ University of Chinese Academy of Sciences, Beijing 100049, China

⁷ School of Pharmaceutical Sciences, Guizhou Medical University, Guiyang 550025, China

⁸ Pharmacology Laboratory, Zhongshan Traditional Chinese Medicine Hospital, Guangzhou University of Chinese Medicine, Zhongshan 528401, China



Background

The *human Ether-a-go-go Related Gene* channel (hERG) is expressed as the rapidly activating delayed rectifier potassium current (I_{Kr}) in cardiac myocytes, and it plays a critical role in the repolarization of the action potential (AP) of ventricular cardiomyocytes [1]. The deficiency of hERG is usually associated with long-QT syndrome type-2 (LQT2), featured by a prolongation of the QT interval of the surface electrocardiogram (ECG) and T-wave abnormalities [2, 3]. hERG is a depolarization-activated potassium channel, characterized by an extremely fast and atypical C-type inactivation [1, 4–6]. Channels will conduct potassium when hERG is in an activated state, but will not conduct ions when it is in an inactivated state and a closed state [1, 6]. Because hERG activation is slow relatively than rapid inactivation, its current-voltage (I - V) curve is demonstrated as a bell-shaped relationship [1, 6].

hERG belongs to the cyclic nucleotide-binding domain (CNBD) clade of the voltage-gated potassium channel (Kv) superfamily, which contains hyperpolarization-activated and cyclic nucleotide-gated (HCN) channels as well [7]. Both hERG and HCN channels share a similar architecture with a centrally-located pore flanked by four identical subunits [6, 8, 9]. Each channel is a homotetramer, composed of four subunits. Each subunit consists of 6 transmembrane helices (S1-S6), in which S1-S4 is the voltage-sensing domain (VSD), S5-S6 is the pore domain (PD), and the carboxy-terminal is the cyclic nucleotide-binding domain (CNBD) [6, 8, 9]. The S4-S5 linker determines the coupling between VSD and PD [1, 10, 11]. Upon depolarization, the S4 helix will translate along its axis outwardly and move across the membrane [12–15]. This gating motion of the four VSDs can drive the conformational changes in the coupling machinery of the S4-S5 linker that opens the channel's gate eventually [11, 12, 15, 16]. Despite these structural similarities between hERG and HCN channels, hERG is activated by membrane depolarization whereas HCN channels are activated by hyperpolarization [6, 8, 9]. It is a mystery that how channel proteins with such high homology are elicited by completely different membrane voltages (depolarization vs. hyperpolarization) and mediate opposite currents. Since hERG and HCN channels have evolved from the same ancestor [7], it might be reasonable to speculate the structural basis for opposite gating polarity could be subtle and may lie in variations of several amino acid residues. However, the structural basis for the different voltage dependence between hERG and HCN channels is still largely unknown.

The PD of hERG contains all the molecular elements necessary for potassium conduction and for activation and inactivation gating. Activation is classically

associated with conformational rearrangements at the inner helix bundle (the activation gate) whereas C-type inactivation involves structural changes at the selectivity filter (the inactivation gate) [1, 11, 17]. The motion of the S4 helix drives the activation gate through the S4-S5 linker at the intracellular surface and modulates the inactivation gate through the S1-S4 near the extracellular surface [15, 18–25]. Converting the depolarization-activated channel of hERG into a hyperpolarization-activated channel can be achieved by mutating a single residue in either the S4-S5 linker [23, 26] or the S6 helix [27]. D540K of hERG is a well-known channel that carries the reactivated inward current induced by hyperpolarization [23, 26]. Proline substitution of V659 (V659P) within the S6 helix of hERG also passes inward non-deactivating current upon hyperpolarization [27]. The conductance-voltage (G - V) relationship of both the D540K and V659P channel exhibits an increased conductance upon hyperpolarization, which is well described by a Boltzmann function with a $V_{1/2}$ around -100 mV (-117 mV for D540K [26], and -99.7 mV for V659P [27]). For hERG and several other depolarization-activated ion channels [28, 29], the polarity of ion channel gating can be determined by the pore domain as well.

In this study, we found the voltage-sensing domain also plays a critical role in modulating the gating polarity of hERG. An LQT2-related mutant on the S4 helix, K525N [30], mediated an inwardly rectifying non-deactivating current upon hyperpolarization. K525N perturbed pore gate closure and preserved the open and inactivated state. Interestingly, K525N together with either F627Y (K525N&F627Y) or hERG blockers, created a hyperpolarization-activated channel with $V_{1/2}$ is about -103.2 mV. K525N&F627Y was still inhibited by pore blockers, dofetilide, and E4031. Moreover, we found that a potential extracellular interaction between the S1 helix and the S5-P region is critical for the hyperpolarization-activation channel of K525N&F627Y.

Results

K525N&F627Y is a hyperpolarization-activated channel

We chose to use hERG as a model channel, to explore the role of the voltage-sensing domain in modulating its rectification property. On transfection with hERG cDNA, CHO-K1 cells expressed a large potassium current with biophysical properties reminiscent of the I_{Kr} current in cardiomyocytes [6] (Fig. 1a). A slowly activating potassium current developed during depolarizations above -60 mV with maximum at a potential 0 mV in hERG-expressing cells (Fig. 1b). It opens with evident inactivation at more positive potential (Fig. 1a, and b). Analysis of the tail current allowed us to characterize the half-activation voltage ($V_{1/2}$) which is -18.7 ± 1.1 mV (Fig. 1c, and i). The

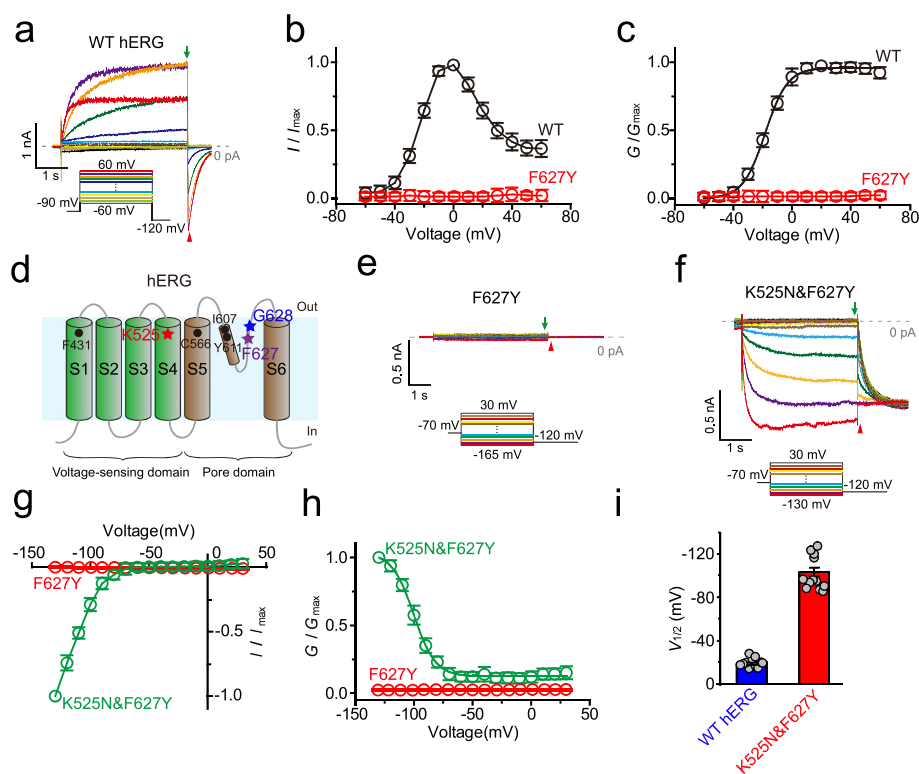


Fig. 1 K525N&F627Y is a hyperpolarization-activated channel. **a** Representative currents of WT hERG overexpressed in CHO cells. The step voltage protocol (below) varies from -60 to +60 mV with a holding potential of -90 mV. The green arrow and red arrowhead indicate the measurement region of outward currents and tail currents, respectively. The 0 pA is indicated by a dashed line. **b** The normalized current-voltage (I - V) curve of WT hERG ($n \geq 6$) and F627Y ($n \geq 6$). Measured currents are indicated by the green arrow in Fig. 1a. **c** The normalized conductance-voltage (G - V) curve of WT hERG ($n \geq 6$). Measured currents are indicated by the red arrowhead in Fig. 1a. **d** Diagram of an hERG channel subunit that can be divided into a VSD (S1-S4) and a PD (S5-S6). K525 in the S4 helix and F627 in the selective filter is indicated by a red and purple star, respectively. The potential interacting residues (F431, C566, I607, and Y611) are also labelled with black dots. F431 is in S1, C566 is in S5, I607 and Y611 are in the pore helix. **e** Representative currents of F627Y. Step voltage protocol (below) varies from -165 to +30 mV with a holding potential at -70 mV. **f** Representative currents of K525N&F627Y. Step voltage protocol (below) varies from -130 to +30 mV with a holding potential at -70 mV. **g** The normalized I - V curve ($n \geq 6$) and **h** The normalized G - V curve ($n \geq 6$) of K525N&F627Y. **i** $V_{1/2}$ values of WT hERG and K525N&F627Y ($n = 12$). Error bars represent mean \pm SEM

C-type inactivation gate of hERG contains ${}_{626}\text{GFG}_{628}$ motif in the selectivity filter [4, 5]. As one of the key determinants of C-type inactivation, F627 regulates the asymmetrical constricted-like conformation of the selectivity filter [4] (Fig. 1d). The tyrosine substitution of F627 (F627Y) leads to an ion non-conducting channel under physiological solutions (Fig. 1a-e), consistent with previous studies [4, 31–33].

We investigated channel properties of many double mutants that combined mutations of gating charge and F627Y (Fig. 1d). To our surprise, the nonfunctional single mutant of F627Y was rescued by the K525N mutation (Fig. 1f). Moreover, K525N&F627Y was activated by membrane hyperpolarization and mediated non-deactivated inward current (Fig. 1f-h, and Additional file 1: Fig. S1), in stark contrast to the wild-type (WT) hERG that was activated by membrane depolarization

and conducted outward current (Fig. 1a, and b). Such behavior is reminiscent of the hyperpolarization-induced activation of D540K [23, 26] and V659P [27] of hERG, W434F-P475D of Shaker-IR [34], L226P of NachBac [28], and L271P&D312N of SKOR [29]. We observed K525N&F627Y was completely closed at physiological membrane potentials and began to conduct a slowly activated inward current as the membrane voltage was changed from -70 to -135 mV (Fig. 1f, g, and Additional file 1: Fig. S1). Such activation properties are exactly opposite to those of WT hERG, which was activated by more positive membrane potentials (Figs. 1a, and b; from -60 to +60 mV). The voltage dependence of the peak tail current for K525N&F627Y was fitted to a Boltzmann function, yielding a $V_{1/2}$ of -103.2 ± 4.1 mV (Fig. 1h, and i), 84.5 mV more negative than that for WT (Fig. 1i). Also, K525N&G628S is a hyperpolarization-activated channel

similar with K525N&F627Y (Additional file 1: Fig. S1). The gating polarity of K525N&F627Y and K525N&G628S is reversed to WT hERG (Fig. 1c, h, and Additional file 1: Fig. S1).

Under physiological solutions (external: 5 mM K^+ and 140 Na^+ versus internal: 145 mM K^+), the reversal potential of WT hERG and K525N&F627Y was around -60 mV (Additional file 2: Fig. S2); and it changed to about 0 mV (Additional file 2: Fig. S2) while symmetric potassium solutions were applied (external and internal: 145 mM K^+). Therefore, the reversal potential of WT hERG and K525N&F627Y was strictly determined by the potassium gradient between the extracellular (external) solution and intracellular (internal) solution. K525N&F627Y and K525N&G628S remained a potassium channel with a limited permeability to sodium and NMDG (Figs. 2a, and Additional file 2: Fig. S2), which is similar to WT hERG (Fig. 2b).

K525N&F627Y is inhibited by hERG channel blockers

hERG channel physiologically conducts ions through the alpha (α) pore [6]. However, the omega (Ω) pore would be created by mutating some gating charges in the S4 of voltage-gated ion channels, especially the first gating charge [35–37]. K525S has been reported that it can create an extra Ω pore in hERG [38]. Therefore, a question is raised on whether the hyperpolarization-activated conductance of K525N&F627Y is indeed carried by the hERG channel, and if true, whether it is still carried by the α pore. To address these questions, we first investigated the K525N&F627Y current sensitivity to some hERG channel blockers. Dofetilide and E4031 are both classical blockers through sitting in the central cavity of the α pore [39–41]. We found that both dofetilide (Fig. 3a–c) and E4031 (Fig. 3d–f) also significantly inhibited the inward current of K525N&F627Y. The sensitivity of K525N&F627Y to both blocker is dramatically reduced compared with wild-type hERG, which might be attributed to an inability of the open gate to trap blockers in

the pore at hyperpolarized potentials [40]. The similar phenomenon was also observed for the D540K mutant [40]. The G - V curve of K525N&F627Y was dramatically left-shifted in the presence of either dofetilide (Fig. 3g–i) or E4031 (Fig. 3j–l). Given that dofetilide and E4031 often act as blocker binding in the α pore [39, 41], and the K525N&F627Y channel shares the same ion selectivity and permeability as the WT hERG channel (Figs. 2, and Additional file 2: Fig. S2), it is reasonable to speculate the inward current of K525N&F627Y is still through the α pore as WT hERG.

K525N perturbs the channel closed state, presents an open and an inactivated state

To explore the hyperpolarization-activated gating mechanism of K525N&F627Y, we characterized the channel properties of K525N. K525 is proximate to the S3-S4 linker that regulates hERG activation gate [42, 43]. Unlike WT hERG, K525N produced an instantaneous current that was observed upon hyperpolarization as well as depolarization (Fig. 4a, and d). K525N still exhibited properties of a depolarization-activated channel, and tail currents at -150 mV were progressively larger as if the membrane potential was depolarized (Fig. 4a, b, and Additional file 3: Fig. S3). The tail current demonstrated compromised deactivation, and half of the maximum conductance remained at -150 mV (Fig. 4a, and b). K525N can not be fully closed even if the voltage is -170 mV (Fig. 4a, and b). The G - V curve of K525N is dramatically left-shifted compared with WT hERG (Fig. 4b), giving a $V_{1/2}$ of -95.6 ± 3.9 mV and -19.3 ± 2.1 mV for K525N and WT, respectively (Fig. 4c). An inwardly rectifying current was still detected at more positive potentials (-46.2 ± 3.9 mV) with a maximum current recorded at more negative potentials than WT hERG (6.0 ± 0.8 mV) (Fig. 4d–f). With further depolarization, the current of K525N amplitude decreased progressively (Fig. 4d, and e), which is due to the channel voltage-dependent inactivation. Thus, K525N perturbed channel closure and

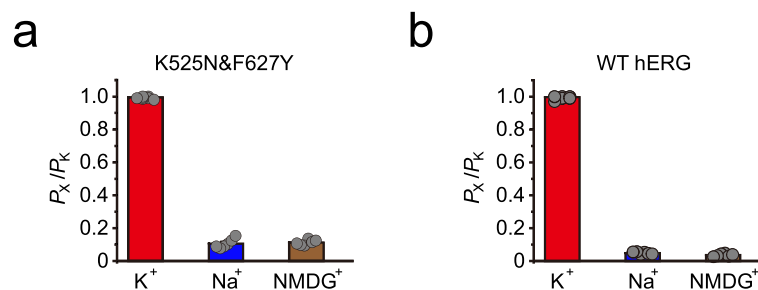


Fig. 2 K525N&F627Y is a K^+ selective channel. **a** Analysis of relative K^+ permeability over Na^+ , or $NMDG^+$ of K525N&F627Y based on E_{rev} measurement ($n \geq 6$). **b** Analysis of relative K^+ permeability over Na^+ , or $NMDG^+$ of WT hERG based on E_{rev} measurement ($n \geq 6$). Error bars represent mean \pm SEM

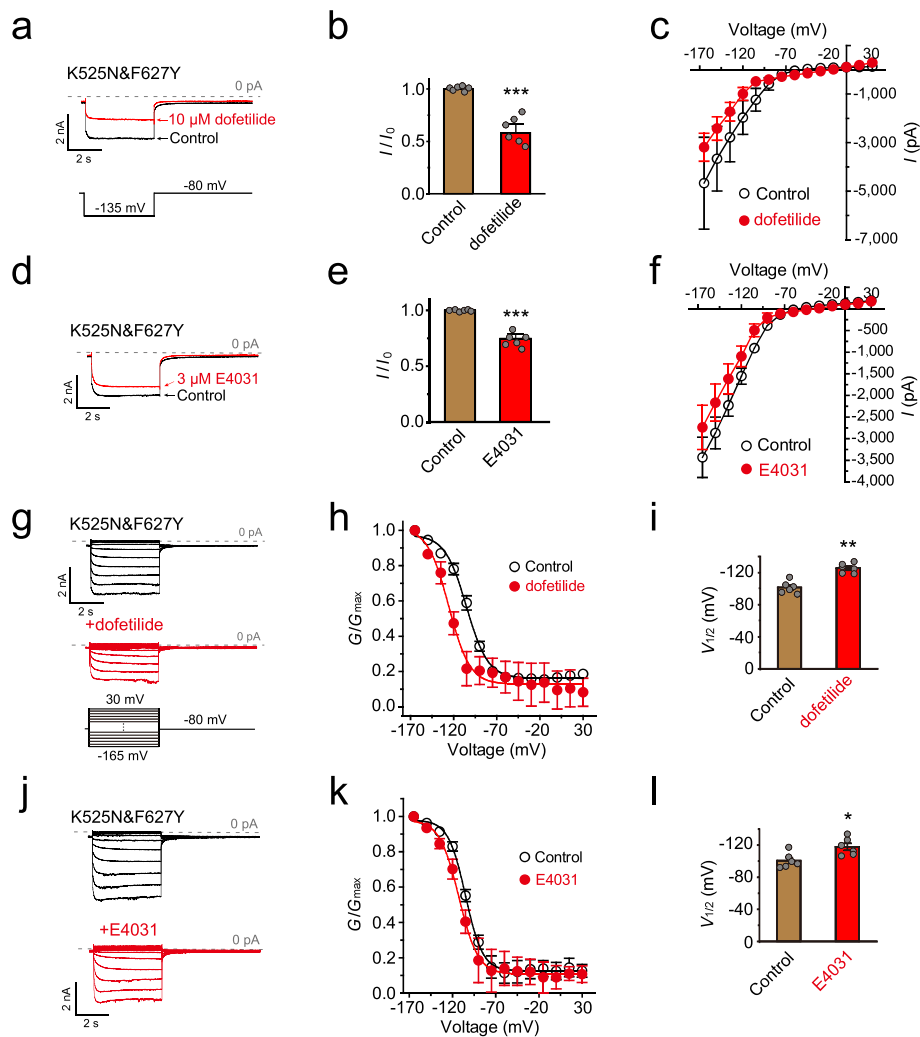


Fig. 3 K525N&F627Y is inhibited by dofetilide and E4031. **a** Representative currents of K525N&F627Y with or without 10 μM dofetilide. Inward currents were elicited with -135 mV (the protocol see below). **b** histogram of I/I_0 at -135 mV with or without dofetilide ($n \geq 6$). **c** I - V curves of K525N&F627Y with or without dofetilide ($n \geq 6$). **d** Representative currents of K525N&F627Y with or without 3 μM E4031. **e** histogram of I/I_0 at -135 mV with or without E4031 ($n \geq 6$). **f** I - V curves of K525N&F627Y with or without E4031 ($n \geq 6$). **g** Representative step currents of K525N&F627Y with or without dofetilide. The step voltage protocol (below) varies from -165 to $+30$ mV. **h** The G - V curve ($n \geq 6$) and **i** $V_{1/2}$ values ($n \geq 6$) of K525N&F627Y with or without dofetilide. **j** Representative step currents of K525N&F627Y with or without E4031. **k** The G - V curve ($n \geq 6$) and **l** $V_{1/2}$ values ($n \geq 6$) of K525N&F627Y with or without E4031. Error bars represent mean \pm SEM. * $P < 0.05$, ** $P < 0.01$; *** $P < 0.001$, two-tailed Student's t -test

preserved the channel activation state and inactivation state.

The gating polarity of K525N is pharmacologically reversed by E4031 and cisapride

Both E4031 and cisapride bind in the central cavity of the PD near the inactivation gate of hERG channel [39, 41, 44]. To further explore the role of the inactivation in the gating polarity of hERG, we studied the influence of E4031 and cisapride on the channel properties of K525N. In the presence of E4031 at 3 μM ($> IC_{100} = 1 \mu\text{M}$ on WT hERG in CHO cells [45]) and Cisapride at 10 μM ($> IC_{100}$

$= 1 \mu\text{M}$ on WT hERG in CHO cells [46]), the outward current was almost completely blocked (Fig. 5a, and d). However, a partial inward current of K525N remained (Fig. 5a, and d), showing the peak current was more sensitive to E4031 and cisapride than the steady-state current (Fig. 5b, c, e, and f). The residual inward current (Fig. 5a, and d) is reminiscent of that of K525N&F627Y (Fig. 1f). The tail current of the residual inward current was increased as the membrane potential decreased from -100 mV (Fig. 5g, and h). The G - V curve can be fitted by a Boltzmann function with the $V_{1/2}$ of -147.0 ± 12.7 mV and -119.6 ± 5.4 mV for K525N with E4031 and cisapride,

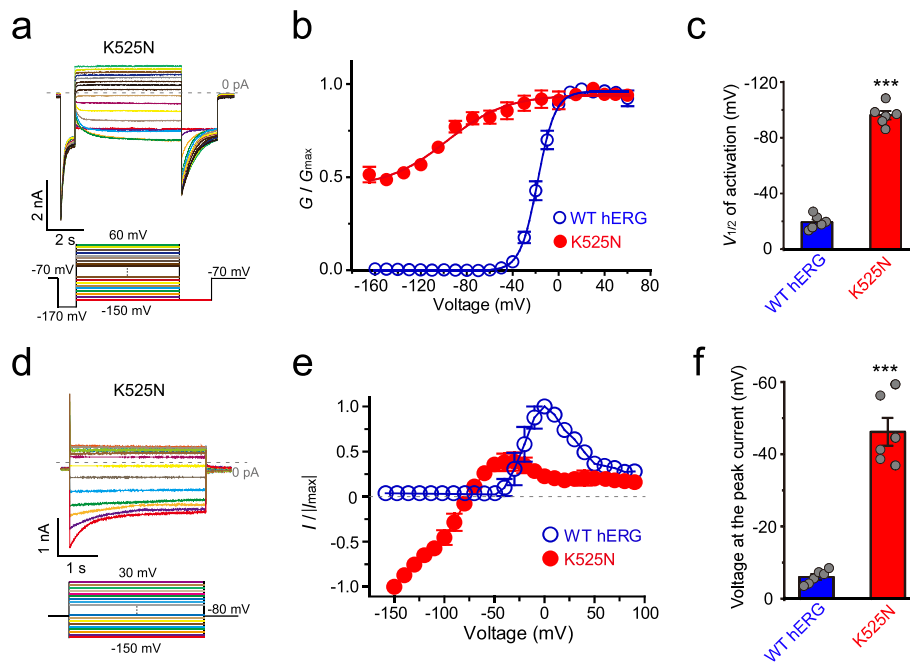


Fig. 4 K525N perturbs the channel closure and preserves the open and inactivated state. **a** Representative step currents of K525N elicited with a complicated protocol. The step voltage protocol (below) varies from -150 to +60 mV with a holding potential of -70 mV. Since channels were instantaneously open at -70 mV, a -170 mV was applied before the step trying to close the pore gate and to detect the activation kinetics. A -150 mV followed the step to detect tail currents. **b** The G-V curve (n≥6) and **c** $V_{1/2}$ of activation values (n≥6) of K525N. **d** Representative step currents of K525N elicited with an easier protocol. The step voltage protocol (below) varies from -150 to +60 mV. **e** The G-V curve (n≥6) and **f** the voltage at the peak current (n≥6) of K525N. Error bars represent mean ± SEM. *** $P < 0.001$, two-tailed Student's t-test

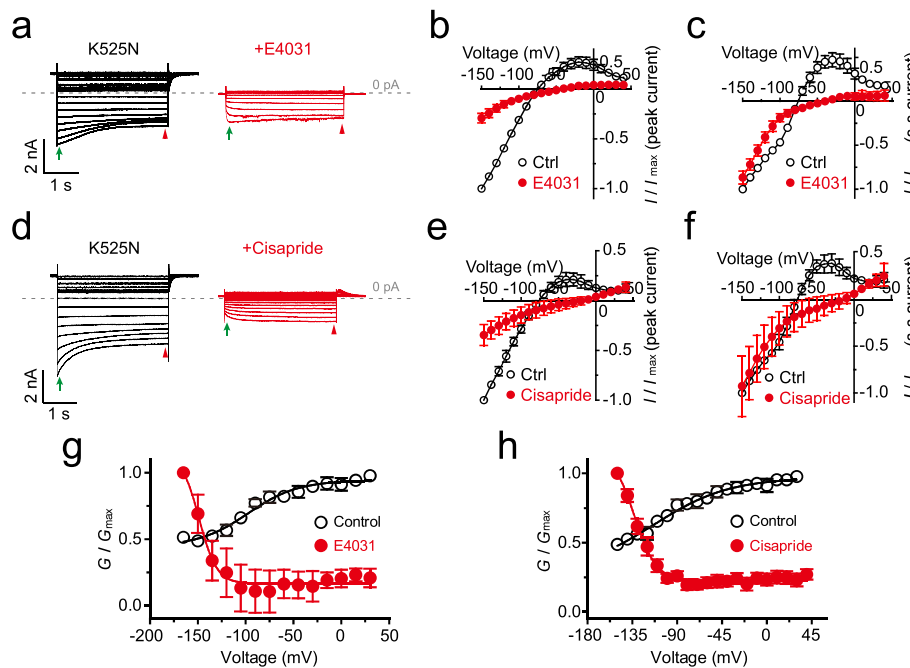


Fig. 5 The gating polarity of K525N is switched by E4031 and cisapride. **a** Representative step currents of K525N with or without 3 μM E4031. Green arrows indicate peak currents, and red arrowheads indicate steady-state currents. **b** I - V curves of peak currents (n≥6) and **c** steady-state currents (n≥6) of K525N with or without E4031. **d** Representative step currents of K525N with or without 10 μM cisapride. Green arrows indicate peak currents, and red arrowheads indicate steady-state currents. **e** I - V curves of peak currents (n≥6) and **f** steady-state currents (n≥6) of K525N with or without cisapride. G-V curves of K525N with or without **g** E4031 and **h** cisapride. Error bars represent mean ± SEM

respectively (Fig. 5g, and h). E4031 and cisapride converted a depolarization-activated channel of K525N into a hyperpolarization-activated channel.

The extracellular interaction between the VSD and PD is critical for functions of K525N&F627Y

The extracellular and intracellular interaction of the voltage-sensing domain and the pore domain regulate voltage-gated ion channel functions including the hERG channel [18, 20, 22, 24, 25, 47]. The VSD-PD interaction is the mechanism that confers voltage-dependent inactivation in hERG, and whether the hyperpolarization channel of K525N&F627Y can be regulated by the extracellular interaction of the VSD and the pore is not clear. Based on the cryo-EM structure of hERG (PDB:5VA1) [6], we observed the extracellular interaction is potentially composed of the F431 on

the S1, C566 in the S5, I607, and Y611 on the pore helix [6, 19, 22] (Fig. 6a). These potential interaction sites are flanked by K525 in the S4 and F627 in the selective filter (Fig. 6a). Mutating F431, C566, I607, and Y611 to the alanine with K525N&F627Y background did not change the expression pattern of hERG on the plasma membrane (Additional file 4: Fig. S4). With mutations of F431A, C566A, and Y611A, K525N can not rescue the current of F627Y at all. The mutation of I607A also partially disrupted the rescue effect of K525N on F627Y, and the inward current of K525N&F627Y&I607A was significantly reduced (Fig. 6b-d). Mutations of other residues beyond this region, such as I409A, barely affected functions of K525N&F627Y (Additional file 4: Fig. S4). F431A, C566A, and Y611A eliminated the current of K525N as well (Additional file 4: Fig. S4). Therefore, the potential interaction between the VSD and

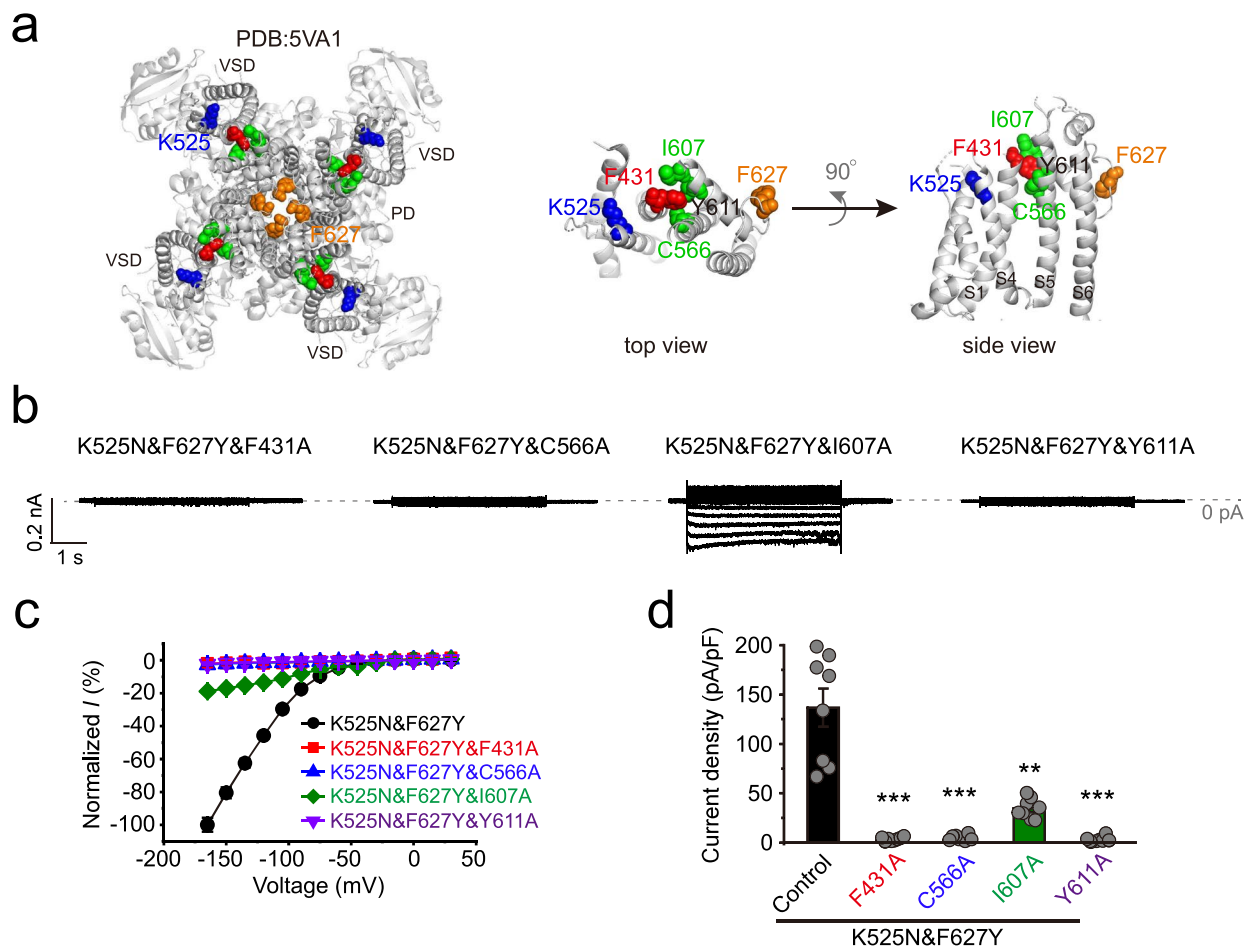


Fig. 6 F431A, C566A, I607A, and Y611A impair the inward current of K525N&F627Y. **a** The cryo-EM structure of hERG (PDB: 5VA1) [6] highlighted with K525 (blue), F627 (yellow), and potential key residues (red in the S1 helix, and green in the S5-P region) of the extracellular interaction face between the VSD and the PD. The top view and side view of the interaction region are zoomed out and shown in the *Right* panel. **b** Representative step currents of F431A, C566A, I607A, and Y611A on top of K525N&F627Y, respectively. **c** Normalized *I-V* curves ($n \geq 6$) and **d** current density ($n \geq 6$) of F431A, C566A, I607A, and Y611A on top of K525N&F627Y, respectively. Error bars represent mean \pm SEM. ** $P < 0.01$; *** $P < 0.001$, two-tailed Student's *t*-test

PD is also involved in the hyperpolarization-activated properties of K525N&F627Y.

K525N&S631A is a “leak” channel

Previously, S631A was reported as an “inactivation-alleviation” mutant [48, 49]. Consistently, we found that the inactivation was absent even at +50 mV in S631A [48, 49] (Fig. 7a, and c). We first combined S631A with K525N to

create K525N&S631A and recorded the channel behavior at a large range of membrane potentials (Fig. 7b). Interestingly, K525N&S631A was a “leak” channel with substantial inward and outward currents (Fig. 7b, and c). The inward current of K525N&S631A was different from K525N, as a saturated current was achieved at negative potentials (Fig. 7b, and c). However, K525N&S631A is still a depolarization-activated channel with the voltage

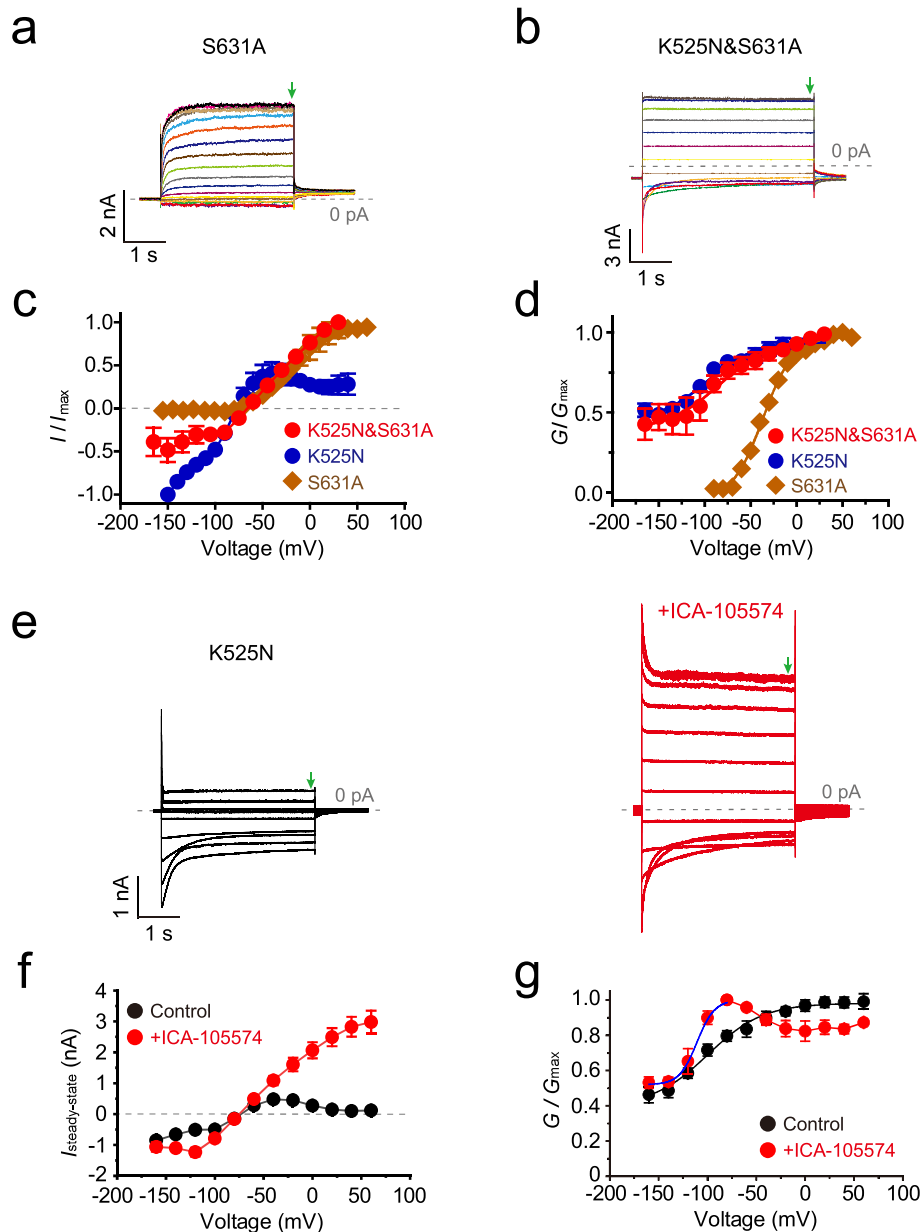


Fig. 7 K525N&S631A is a “leak” channel. **a** Representative step currents of S631A, and **b** K525N&S631A. **c** I - V curves (n ≥ 6) of S631A, K525N, and K525N&S631A, respectively. Steady-state currents indicated by green arrows in Fig. 7a and b were quantified. **d** G - V curves of S631A, K525N, and K525N&S631A, respectively. **e** Representative step currents and **f** I - V curves (n ≥ 6) of K525N with or without 10 μM ICA-105574. **g** G - V curves of K525N with or without 10 μM ICA-105574. In the presence of ICA-105574, the G - V curve was fitted by the Boltzmann equation (blue line). Error bars represent mean ± SEM

dependence similar to K525N (Fig. 7d). ICA-105574 is a potent activator of hERG by alleviating the inactivation [50–52]. In the presence of ICA-105574, K525N also behaved as a “leak” channel (Fig. 7e), and the inward current was saturated at negative potential as well (Fig. 7f). ICA-105574 left-shifted the *G*-*V* curve of K525N channel at potential more negative than -80 mV significantly (Fig. 7g). Thus, the VSD and the PD together could also reshape hERG to a “leak” channel.

Discussion

The VSD is involved in switching the gating polarity of hERG

Both hERG and HCN belong to CNBD-family channels, sharing a similar structure [6, 8, 9]. Recently, several studies have revealed that the structural basis for the different polarities of the depolarization-activated channel and hyperpolarization-activated channel is associated with the pore domain of hERG [23, 26, 27]. D540K in the S4-S5 linker [23, 26] and V659P in the S6 helix [27] of hERG mediate the inward current that is gradually larger as if the membrane potential decreases. K540 interacts with R665 in the S6 helix to couple the VSD with the PD, underlying the mechanism of hyperpolarization-dependent opening of D540K [23]. V659P introduces a kink that disrupts the coupling between the VSD and the PD [27]. In the Shaker channel, the combination of L434F and P475D, two residues in the PD, converts it to the hyperpolarization activated channel as well [34]. Whether the VSD is involved in determining the gating polarity of hERG? In HCN-EAG chimera channels, the substitution of serine in helix breaking transition in the S4 with a bulky hydrophobic amino acid flips the gating polarity from inward to outward-rectifying [53], suggesting the VSD may be critical to the gating polarity. The S3-S4 linker is important for stabilizing the closed conformation of hERG relative to the open state [42, 43, 54]. As the first gating charge, K525 stabilizes the closed state of hERG. Mutations of K525 would disturb the pore gate closure, and left-shift the voltage dependence dramatically [43, 54–58]. We found herein K525N also impairs the pore gate closure and preserves the open and inactivated state. When cooperating with F627Y, a mutation in the inactivation gate [4, 31, 32], K525N successfully inverted the polarity of voltage dependence (Fig. 1e-h). Therefore, the VSD is also involved in modulating the gating polarity of hERG.

The hyperpolarization-activated mechanism of K525N&F627Y

The PD of the hERG channel contains the intracellular activation and extracellular inactivation gate [6]. Both gates are intimately regulated by the VSD (Fig. 8a) [6]. In

the closed state at the rest membrane potential, the voltage sensor is located intracellularly, leading to the activation gate being closed and the inactivation gate being open [1, 6, 11]. Upon depolarization, the voltage sensor slides outwardly, inducing the activation gate to gradually open (Fig. 1a, and c) via the intracellular S4-S5 linker. Whereas the inactivation gate would keep open at a voltage lower than 0 mV, and close at higher voltages (Fig. 1a, and b). How the gating polarity of hERG is reversed in K525N&F627Y? K525 is the first gating charge of hERG [6], and eliminating the first gating charge may prohibit S4 from sliding down completely at hyperpolarization and prevent full closure of the activation gate [13, 59]. Since K525N left-shifts the voltage dependence significantly and eliminates the closed state of the channel (Fig. 4a, and b), the S4 might be located extracellularly, preventing full closure of the activation gate and resulting in a “leaky open” state in K525N&F627Y (Fig. 8b). The inactivation gate may still open at hyperpolarizing potentials, resembling the Shaker-IR-L434F-P475D channel [34]. However, as the membrane potential depolarizes, the inactivation gate gradually close (Fig. 8). K525N&F627Y only exhibits the open and the inactivated state without the closed state. Therefore, it is the inactivation gate that determines the ion conductance of K525N&F627Y, which is reminiscent of the Shaker-IR-L434F-P475D channel [34], and the voltage-dependent gate in the MthK potassium channel [60].

Non-covalent interactions of the VSD and PD in Kv channels

Two tetrameric architectures identified amongst Kv channels: domain-swapped channels, such as Shaker, Kv1.2, and Kv7.1, and non-domain-swapped channels, such as hERG, HCN, and KvAP [6]. In domain-swapped channels, the VSD from one subunit is in close contact with the PD from the adjacent subunit, forming an extensive inter-subunit non-covalent interface. In non-domain-swapped channels the VSD and PD from the same subunit closely contact with a non-covalent interface as well. The non-covalent interface is located at the extracellular region of the VSD and PD. The non-covalent interface of domain-swapped channels is similar with that of non-domain-swapped channels, which is supported by the Shaker channel [20] and hERG [25]. In Shaker K⁺ channel, the voltage sensor is coupled with the selective filter (VS-SF coupling) through the extracellular interaction chain composed of the S4, S5, P-Loop, and SF [20]. The L366H in the S4 restores the K⁺ conduction abrogated by W434F in the PD of the Shaker-IR channel. The disruption of the functional connection between contiguous residues in the S4-S5-(P-Loop)-SF chain is sufficient to decrease the K⁺ conduction of L366H:W434F [20]. A

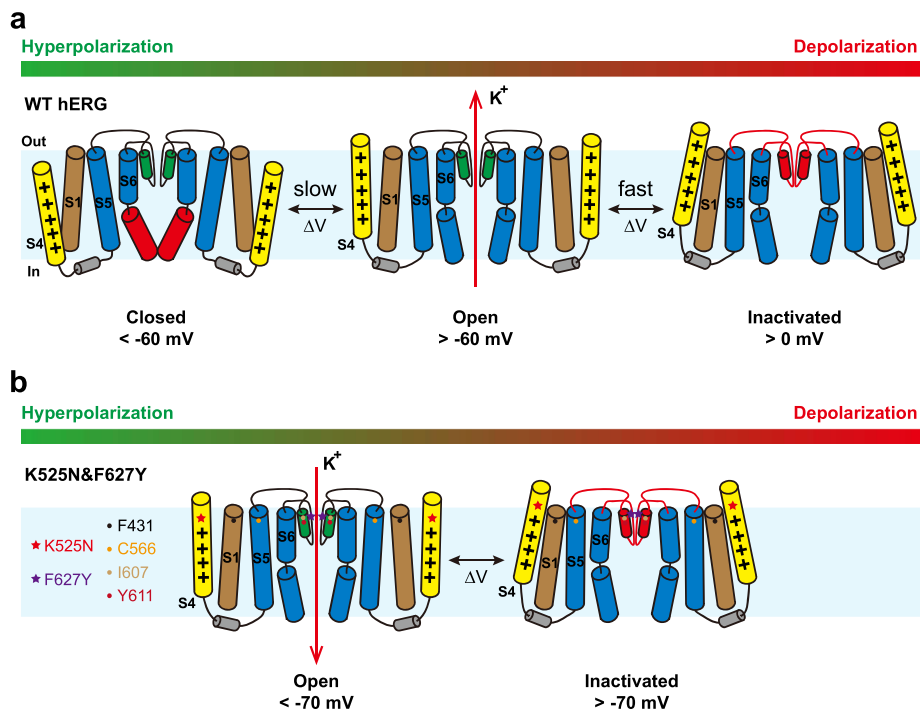


Fig. 8 Suggested model for the inverted gating polarity of K525N&F627Y. **a** Upon depolarization, WT hERG sequentially forms three states, the closed, the open, and the inactivated state. As the membrane potential depolarizes, S4 (yellow) of hERG slides extracellularly and slowly drives the activation gate open (red) via the S4-S5 linker (grey). Channels transit from a closed state into an open state that mediates an outward K⁺ current. Once the membrane potential is higher than 0 mV, S4 further translocates extracellularly, and channels are inactivated. Channels reach the inactivated state that is non-conductive to ions. The non-canonical coupling pathway between the VSD and PD is critical for the hERG channel function. **b** K525N&F627Y preserves two states of hERG, the open and the inactivated state. When the membrane potential is higher than -70 mV, S4 (yellow) usually sits extracellularly. Channels stay in the inactivated state that is non-conductive to ions. Once the membrane potential hyperpolarizes, S4 would translocate mildly toward the intracellular, and relieve the inactivation gate. Channels transit into a “leaky open” state that mediates an inward K⁺ current

kinematic chain of residues that couples the VSD to PD consists of S4/S1 and S1/S5 subunit interfaces in hERG [25]. The movements of VSD electromechanically propagates to the constriction of the SF following the S4-S1-S5-(P-Loop)-SF route relevant for the C-type inactivation [25]. These paths in hERG resemble those for the Shaker channel, suggesting the presence of a common underlying mechanism of electromechanical coupling across the superfamily of Kv channels.

K525N and drug treatment

LQT2-associated mutations broadly distribute in every domain of hERG [2, 30, 61]. A comprehensive study analyzing 226 different LQT mutations reported that 32% resided in transmembrane and pore domains [61]. Deficient protein trafficking to the cell membrane is the dominant mechanism for most of the mutations associated with LQT2 [3, 62]. The trafficking defect mutants can be pharmacologically corrected by culturing in the presence of pore-blocking drugs such as E4031 [62, 63]. Although K525N is still functional on the cell surface (Fig. 4), many

channel functional properties are different from WT hERG. Neither activators nor inhibitors of hERG can restore the functions of K525N (Figs. 5 and 7). Therefore, our study suggests alternative treatments should be developed for LQT2 patients carrying the K525N mutation. In addition, LQT2 syndrome in patients with K525N&R528P [30] may not be pathologically attributed to the K525N, since K525N is a gain-of-function mutant of hERG.

Conclusions

This work characterized the role of a long-QT syndrome type-2-related mutation in the voltage-sensing domain, K525N [30], in modulating the gating polarity of hERG. Completely different from WT hERG, K525N together with F627Y reversed a depolarization-activated channel into a hyperpolarization-activated channel. K525N&F627Y conducted ions upon hyperpolarization and was non-conducted under depolarization. A Boltzmann fitting curve of the tail current gave a $V_{1/2}$ is about -103.2 mV. The non-deactivated

inward current conducted by K525N&F627Y was still sensitive to hERG channel blockers. Pharmacologically, a hyperpolarization-activated channel was also achieved by blocking K525N with E4031 and cisapride. Furthermore, we discovered that the extracellular interaction between the S1 helix and the S5-P region was crucial for the involvement of the VSD in modulating the gating polarity of hERG.

Methods

Mutagenesis

The hERG construct was a gift from M. Sanguinetti (University of Utah), which has been described in our previous work [64]. hERG mutants were generated with QuikChange lightning II site-directed mutagenesis kit (Agilent) and confirmed by DNA sequencing. Primers used for site-directed mutagenesis are listed below.

mutation	Forward primer	Reverse primer
K525N	gatcgggctgctgaacct-gcgcggctg	cagccgcgcagtggtcagcagcccgatc
F627Y	ctcaccagtggtggctacg-gcaactgtctc	gagacgttgccgtagcc-cacactggtgag
G628S	cagtgtgggcttcag-caactgtctctccaac	gttgggagagacggttct-gaagcccacactg
F431A	ccctactcggctgccgccc-tgctgaaggagac	gtctcttcagcagggcg-gcagccgagtaggg
C566A	cgcactgctagccgc-catctgttacgccatc	gatggcgtagcagatggcg-gtagccagtgcg
I607A	ctgggcgccctccgc-caaggacaagtatg	catactgtcttggcg-gaggggcccggccag
Y611A	cctcatcaaggacaa-ggctgtgacggcgctctac	gtagagcgcctgcacagc-cttgccttgatggagg
I419A	catcctgctgctggtcgc-ctacacggctgtcttc	gaagacagccgtgtaggc-gaccagcagcaggatg
S631A	gcttcggcaactgcgctcc-caacaccaac	gttggtgtgggagc-gacgttgccgaagc
K525R	ctgatcgggctgctgcg-gactgcgcggctg	cagccgcgcagtc-cgcagcagcccgatcag
K525C	ctgatcgggctgctgctg-tactgcgcggctgctg	cagcagccgcgcagtagca-cagcagcccgatcag
K525S	gagctgatcgggctgctg-gagtactgcgcggctg	cagccgcgcag-tactcagcagccc-gatcagctc
K525M	gatcgggctgctgatgact-gcgcggc	gccgcgcagtcacagcagc-ccgatc
K525P	gatcgggctgctgctg-cgactgcgcggctg	cagccgcgcagtcg-gcagcagcccgatc
K525A	gatcgggctgctggc-gactgcgcggctg	cagccgcgcagtcg-cagcagcccgatc
K525V	gatcgggctgctggtgact-gcgcggctg	cagccgcgcagtcac-cagcagcccgatc
K525E	ctgatcgggctgctgga-gactgcgcggc	gccgcgcagtcctcagcagc-ccgatcag

Cell culture and transient transfection

Chinese Hamster Ovary (CHO) cells were grown in 50/50 DMEM/F12 (Cellgro, Manassas, VA) with 10% fetal bovine serum (FBS) and 2 mM L-glutamine (Gibco, Carlsbad, CA). To express ion channels, cells were split 24 hours before transfection, plated in 60-mm dishes, and transfected with Lipofectamine 3000™ reagent (Invitrogen, Carlsbad, CA), according to the manufacturer's instruction. At 24 hours after transfection, cells were split and re-plated onto coverslips coated with poly-L-lysine (Sigma-Aldrich, St. Louis, MO). A plasmid for cDNA of GFP (Amara, Gaithersburg, MD) was co-transfected to aid the identification of transfected cells by fluorescence microscopy.

Electrophysiological recording

Whole-cell voltage-clamp recording was carried out at room temperature in CHO cells with an Axopatch-200B amplifier (Molecular Devices, Sunnyvale, CA). The electrodes were pulled from borosilicate glass capillaries (World Precision Instruments, Sarasota, FL). When filled with the intracellular solution, the electrodes had resistances of 3-5 MΩ. The pipette solution contained (mM): KCl 145, MgCl₂ 1, EGTA 5, HEPES 10, and MgATP 5 (pH 7.3 with KOH). During the recording, constant perfusion of the extracellular solution was maintained using a BPS perfusion system (ALA Scientific Instruments, Westbury, NY). The extracellular solution contained (mM): NaCl 140, KCl 5, CaCl₂ 2, MgCl₂ 1.5, HEPES 10, and glucose 10 (pH 7.4 with NaOH). Signals were filtered at 1 KHz and digitized using a DigiData 1550B with pClamp 11.2 software (Molecular Devices, Sunnyvale, CA). Series resistance was compensated by 60-80%.

Determination of relative permeability (P_X/P_K)

The permeability of TMEM175 for Na⁺ and NMDG⁺ relative to K⁺ was estimated based on the Goldman-Hodgkin-Katz current equation [65] and the measured E_{rev} using "bi-ionic" conditions:

$$\frac{P_X}{P_K} = \frac{[K^+]_i e^{(FV/RT)} - [K^+]_e}{[X^+]_e - [X^+]_i e^{(FV/RT)}}$$

Where R, T, F, and V are the gas constant, absolute temperature, Faraday's constant, and the reversal potential, respectively. In the whole-cell recording, the pipette solution is (in mM): KCl 145, EGTA 5, and HEPES 10 (pH 7.3 with KOH). The sodium solution is (in mM): NaCl 145, EGTA 5, and HEPES 10 (pH 7.3 with NaOH). The NMDG solution is (in mM): NMDG 145, EGTA 5, and HEPES 10 (pH 7.3 with HCl). E_{rev} was determined using

a pre-open at 0 mV step protocol in response to extracellular solutions.

Data and statistical analysis

Patch-clamp data were processed using Clampfit 11.2 (Molecular Devices, Sunnyvale, CA), and then analyzed in Origin 2018 (OriginLab, Northampton, MA). Voltage-dependent activation curves were fit with the Boltzmann equation: $G = G_{\min} + (G_{\max} - G_{\min}) / (1 + \exp((V - V_{1/2})/S))$, where G_{\max} is the maximum conductance, G_{\min} is the minimum conductance, $V_{1/2}$ is the voltage for reaching 50% of the maximum conductance and S is the slope factor. Data are presented as means \pm SEM. Significance was estimated using paired two-tailed students' t -tests.

Abbreviations

CNBD	Cyclic nucleotide-binding domain
hERG	human Ether-a-go-go Related Gene
VSD	Voltage-sensing domain
LQT2	Long-QT syndrome type 2
PD	Pore domain
I_{kr}	Rapidly activating delayed rectifier potassium current
ECG	Electrocardiogram
Kv	Voltage-gated potassium channel
HCN	Hyperpolarization-activated and cyclic nucleotide-gated
CHO	Chinese Hamster Ovary
WT	Wild-type

Supplementary Information

The online version contains supplementary material available at <https://doi.org/10.1186/s12915-024-01833-0>.

Additional file 1: Fig. S1. K525N&G628S is a hyperpolarization-activated channel. **a** The expression pattern of hERG-EGFP, and F627Y-EGFP in CHO cells stained with Dil dye (red). **b** The representative ramp current of K525N&F627Y. The ramp protocol (below) ranges from -130 to +30 mV in 5 seconds with a holding potential at -100 mV. **c** Representative currents of G628S. **d** Representative currents of K525N&G628S. **e** The G - V and **e** the I - V curve of K525N&G628S.

Additional file 2: Fig. S2. K525N&G628S is a K^+ selective channel. **a** Representative current traces with ramp protocols and **b** histogram of the reversal potential of K525N&F627Y in the presence of different bath solutions. **c** Representative current traces and **d** histogram of the reversal potential of WT hERG channel in the presence of different bath solutions. **e** Representative current traces and **f** histogram of the reversal potential of K525N&G628S in the presence of different bath solutions. **g** Analysis of relative K^+ permeability over Na^+ , or $NMDG^+$ of K525N&G628S based on E_{rev} measurement ($n \geq 6$). Error bars represent mean \pm SEM.

Additional file 3: Fig. S3. Various K525 mutations disturb channel closure. **a** G - V curves of K525 mutants.

Additional file 4: Fig. 4. I419A did not impair the inward current of K525N&F627Y. **a** The expression pattern of K525N&F627Y&F431A-EGFP, K525N&F627Y&C566A-EGFP, K525N&F627Y&I607A-EGFP, and K525N&F627Y&Y611A-EGFP in CHO cells stained with Dil dye (red). **b** The cryo-EM structure of hERG (PDB: 5VA1) highlighted with K525 (blue), F627 (yellow), and F431 (red) and I419 (green) residues amongst the potential interaction face between the VSD and PD. The top view and side view of the interaction region are zoomed out and shown in the *Right* panel. **c** Representative step currents of K525N&F627Y, and K525N&F627Y&I419A, respectively. **d** Current density ($n \geq 6$) of K525N&F627Y, and K525N&F627Y&I419A, respectively. Representative currents of **e** K525N, **f**

K525N&F431A, **g** K525N&C566A, and **h** K525N&Y611A. Error bars represent mean \pm SEM. ** $P < 0.01$; *** $P < 0.001$, two-tailed Student's t -test.

Acknowledgements

We appreciate the encouragement and helpful comments provided by Dr. P. Li's laboratory and Dr. Z. Gao's laboratory colleagues.

Authors' contributions

Conceptualization: ZL, FT, and PL; Methodology: ZL, FW, HY, and FT; Supervision: ZG, and PL. ZL, FW, FT, CK, TL, and GY performed whole-cell patch-clamp recordings. HY, CY, FH, YL, MT, MP, and MH generated mutants of hERG. FT, ZG, and PL wrote the paper with input from all authors. All authors read and approved the final manuscript.

Funding

This work was supported by grants from the National Natural Science Foundation of China (32100621, 82273913, and 82200368), Guangdong Basic and Applied Basic Research Foundation (2022A1515010851), Zhongshan Municipal Bureau of Science and Technology (220418134367984, and CXTD2022013), China Postdoctoral Science Foundation (2022M713264), Department of Science and Technology of Guangdong Province (2019B090904008, and 2021B0909050003).

Availability of data and materials

All data generated or analyzed during this study are included in this published article and its supplementary information files.

Declarations

Ethics approval and consent to participate

Not applicable.

Consent for publication

Not applicable.

Competing interests

All authors declare no competing financial interests.

Received: 14 February 2023 Accepted: 23 January 2024

Published: 5 February 2024

References

- Vandenberg JI, Perry MD, Perrin MJ, Mann SA, Ke Y, Hill AP. hERG K(+) channels: structure, function, and clinical significance. *Physiol Rev.* 2012;92(3):1393–478.
- Bohnen MS, Peng G, Robey SH, Terrenoire C, Iyer V, Sampson KJ, Kass RS. Molecular Pathophysiology of Congenital Long QT Syndrome. *Physiol Rev.* 2017;97(1):89–134.
- Smith JL, Anderson CL, Burgess DE, Elayi CS, January CT, Delisle BP. Molecular pathogenesis of long QT syndrome type 2. *J Arrhythm.* 2016;32(5):373–80.
- Li J, Shen R, Reddy B, Perozo E, Roux B. Mechanism of C-type inactivation in the hERG potassium channel. *Sci Adv.* 2021;7(5).
- Miranda WE, DeMarco KR, Guo J, Duff HJ, Vorobyov I, Clancy CE, Noskov SY. Selectivity filter modalities and rapid inactivation of the hERG1 channel. *Proc Natl Acad Sci U S A.* 2020;117(6):2795–804.
- Wang W, MacKinnon R. Cryo-EM Structure of the Open Human Ether-a-go-go-Related K(+) Channel hERG. *Cell.* 2017;169(3):422–430 e410.
- James ZM, Zagotta WN. Structural insights into the mechanisms of CNBD channel function. *J Gen Physiol.* 2018;150(2):225–44.
- Lee CH, MacKinnon R. Voltage Sensor Movements during Hyperpolarization in the HCN Channel. *Cell.* 2019;179(7):1582–1589 e1587.
- Lee CH, MacKinnon R. Structures of the Human HCN1 Hyperpolarization-Activated Channel. *Cell.* 2017;168(1–2):111–120 e111.

10. Piper DR, Sanguinetti MC, Tristani-Firouzi M. Voltage sensor movement in the hERG K⁺ channel. *Novartis Found Symp.* 2005;266:46–52 discussion 52–46, 95–49.
11. Cheng YM, Claydon TW. Voltage-dependent gating of HERG potassium channels. *Front Pharmacol.* 2012;3:83.
12. Tombola F, Pathak MM, Isacoff EY. How does voltage open an ion channel? *Annu Rev Cell Dev Biol.* 2006;22:23–52.
13. Jensen MO, Jogini V, Borhani DW, Leffler AE, Dror RO, Shaw DE. Mechanism of voltage gating in potassium channels. *Science.* 2012;336(6078):229–33.
14. Zhang M, Liu J, Tseng GN. Gating charges in the activation and inactivation processes of the HERG channel. *J Gen Physiol.* 2004;124(6):703–18.
15. Smith PL, Yellen G. Fast and slow voltage sensor movements in HERG potassium channels. *J Gen Physiol.* 2002;119(3):275–93.
16. Van Slyke AC, Rezazadeh S, Snopkowski M, Shi P, Allard CR, Claydon TW. Mutations within the S4-S5 linker alter voltage sensor constraints in hERG K⁺ channels. *Biophys J.* 2010;99(9):2841–52.
17. Flynn GE, Zagotta WN. Insights into the molecular mechanism for hyperpolarization-dependent activation of HCN channels. *Proc Natl Acad Sci U S A.* 2018;115(34):E8086–95.
18. Lee SY, Banerjee A, MacKinnon R. Two separate interfaces between the voltage sensor and pore are required for the function of voltage-dependent K⁽⁺⁾ channels. *PLoS Biol.* 2009;7(3):e47.
19. Phan K, Ng CA, David E, Shishmarev D, Kuchel PW, Vandenberg JJ, Perry MD. The S1 helix critically regulates the finely tuned gating of Kv11.1 channels. *J Biol Chem.* 2017;292(18):7688–705.
20. Bassetto CA, Carvalho-de-Souza JL, Bezanilla F. Molecular basis for functional connectivity between the voltage sensor and the selectivity filter gate in Shaker K⁽⁺⁾ channels. *Elife.* 2021;10.
21. Vardanyan V, Pongs O. Coupling of voltage-sensors to the channel pore: a comparative view. *Front Pharmacol.* 2012;3:145.
22. Colenso CK, Sessions RB, Zhang YH, Hancox JC, Dempsey CE. Interactions between Voltage Sensor and Pore Domains in a hERG K Channel Model from Molecular Simulations and the Effects of a Voltage Sensor Mutation. *J Chem Inf Model.* 2013;53.
23. Tristani-Firouzi M, Chen J, Sanguinetti MC. Interactions between S4-S5 linker and S6 transmembrane domain modulate gating of HERG K⁺ channels. *J Biol Chem.* 2002;277(21):18994–9000.
24. Liu J, Zhang M, Jiang M, Tseng GN. Structural and functional role of the extracellular s5-p linker in the HERG potassium channel. *J Gen Physiol.* 2002;120(5):723–37.
25. Bassetto CAZ Jr, Costa F, Guardiani C, Bezanilla F, Giacomello A. Non-canonical electromechanical coupling paths in cardiac hERG potassium channel. *Nat Commun.* 2023;14(1):1110.
26. Sanguinetti MC, Xu QP. Mutations of the S4-S5 linker alter activation properties of HERG potassium channels expressed in *Xenopus* oocytes. *J Physiol.* 1999;514(Pt 3):667–75.
27. Thouta S, Sokolov S, Abe Y, Clark SJ, Cheng YM, Claydon TW. Proline scan of the HERG channel S6 helix reveals the location of the intracellular pore gate. *Biophys J.* 2014;106(5):1057–69.
28. Zhao Y, Scheuer T, Catterall WA. Reversed voltage-dependent gating of a bacterial sodium channel with proline substitutions in the S6 transmembrane segment. *Proc Natl Acad Sci U S A.* 2004;101(51):17873–8.
29. Li L, Liu K, Hu Y, Li D, Luan S. Single mutations convert an outward K⁺ channel into an inward K⁺ channel. *Proc Natl Acad Sci U S A.* 2008;105(8):2871–6.
30. Millat G, Chevalier P, Restier-Miron L, Da Costa A, Bouvagnet P, Kugener B, Fayol L, Gonzalez Armengod C, Oddou B, Chanavat V, et al. Spectrum of pathogenic mutations and associated polymorphisms in a cohort of 44 unrelated patients with long QT syndrome. *Clin Genet.* 2006;70(3):214–27.
31. Pettini F, Domene C, Furini S. Early Steps in C-Type Inactivation of the hERG Potassium Channel. *J Chem Inf Model.* 2023;63(1):251–8.
32. Gang H, Zhang S. Na⁺ permeation and block of hERG potassium channels. *J Gen Physiol.* 2006;128(1):55–71.
33. Zhao Y, Wang T, Guo J, Yang T, Li W, Koichopolos J, Lamothe SM, Kang Y, Ma A, Zhang S. Febrile temperature facilitates hERG/IKr degradation through an altered K⁽⁺⁾ dependence. *Heart Rhythm.* 2016;13(10):2004–11.
34. Coonen L, Martinez-Morales E, Van De Sande DV, Snyders DJ, Cortes DM, Cuello LG, Labro AJ. The nonconducting W434F mutant adopts upon membrane depolarization an inactivated-like state that differs from wild-type Shaker-IR potassium channels. *Sci Adv.* 2022;8(37):eabn1731.
35. Jurkat-Rott K, Groome J, Lehmann-Horn F. Pathophysiological role of omega pore current in channelopathies. *Front Pharmacol.* 2012;3:112.
36. Jiang D, Gamal El-Din TM, Ing C, Lu P, Pomes R, Zheng N, Catterall WA. Structural basis for gating pore current in periodic paralysis. *Nature.* 2018;557(7706):590–4.
37. Moreau A, Gosselin-Badarouine P, Chahine M. Biophysics, pathophysiology, and pharmacology of ion channel gating pores. *Front Pharmacol.* 2014;5:53.
38. Kudaibergenova M, Guo J, Khan HM, Lees-Miller J, Mousaei M, Miranda W, Ngo VA, Noskov SY, Tieleman DP, Duff HJ. The voltage-sensing domain of a hERG1 mutant is a cation-selective channel. *Biophysical J.* 2022;121(23):14.
39. Perry M, Sanguinetti M, Mitcheson J. Revealing the structural basis of action of hERG potassium channel activators and blockers. *J Physiol.* 2010;588(Pt 17):3157–67.
40. Kamiya K, Niwa R, Mitcheson JS, Sanguinetti MC. Molecular determinants of HERG channel block. *Mol Pharmacol.* 2006;69(5):1709–16.
41. Lees-Miller JP, Duan Y, Teng GQ, Duff HJ. Molecular determinant of high-affinity dofetilide binding to HERG1 expressed in *Xenopus* oocytes: involvement of S6 sites. *Mol Pharmacol.* 2000;57(2):367–74.
42. Choveau FS, El Harchi A, Rodriguez N, Louerat-Oriou B, Baro I, Demolombe S, Charpentier F, Loussouarn G. Transfer of rolf S3-S4 linker to HERG eliminates activation gating but spares inactivation. *Biophys J.* 2009;97(5):1323–34.
43. Dou Y, Goodchild SJ, Velde RV, Wu Y, Fedida D. The neutral, hydrophobic isoleucine at position I521 in the extracellular S4 domain of hERG contributes to channel gating equilibrium. *Am J Physiol Cell Physiol.* 2013;305(4):C468–78.
44. Kamiya K, Niwa R, Morishima M, Honjo H, Sanguinetti MC. Molecular determinants of hERG channel block by terfenadine and cisapride. *J Pharmacol Sci.* 2008;108(3):301–7.
45. McPate MJ, Duncan RS, Witchel HJ, Hancox JC. Disopyramide is an effective inhibitor of mutant HERG K⁺ channels involved in variant 1 short QT syndrome. *J Mol Cell Cardiol.* 2006;41(3):563–6.
46. Walker BD, Singleton CB, Bursill JA, Wyse KR, Valenzuela SM, Qiu MR, Breit SN, Campbell TJ. Inhibition of the human ether-a-go-go-related gene (HERG) potassium channel by cisapride: affinity for open and inactivated states. *Br J Pharmacol.* 1999;128(2):444–50.
47. Butler A, Helliwell MV, Zhang Y, Hancox JC, Dempsey CE. An Update on the Structure of hERG. *Front Pharmacol.* 2019;10:1572.
48. Zou A, Xu QP, Sanguinetti MC. A mutation in the pore region of HERG K⁺ channels expressed in *Xenopus* oocytes reduces rectification by shifting the voltage dependence of inactivation. *J Physiol.* 1998;509(Pt 1):129–37.
49. Schonherr R, Heinemann SH. Molecular determinants for activation and inactivation of HERG, a human inward rectifier potassium channel. *J Physiol.* 1996;493(Pt 3):635–42.
50. Gerlach AC, Stoehr SJ, Castle NA. Pharmacological removal of human ether-a-go-go-related gene potassium channel inactivation by 3-nitro-N-(4-phenoxyphenyl) benzamide (ICA-105574). *Mol Pharmacol.* 2010;77(1):58–68.
51. Zangerl-Plessl EM, Berger M, Drescher M, Chen Y, Wu W, Maulide N, Sanguinetti M, Stary-Weinzinger A. Toward a Structural View of hERG Activation by the Small-Molecule Activator ICA-105574. *J Chem Inf Model.* 2020;60(1):360–71.
52. Garg V, Stary-Weinzinger A, Sachse F, Sanguinetti MC. Molecular determinants for activation of human ether-a-go-go-related gene 1 potassium channels by 3-nitro-n-(4-phenoxyphenyl) benzamide. *Mol Pharmacol.* 2011;80(4):630–7.
53. Kasimova MA, Tewari D, Cowgill JB, Ursuleaz WC, Lin JL, Delemotte L, et al. Helix breaking transition in the S4 of HCN channel is critical for hyperpolarization-dependent gating. *Elife.* 2019;8.
54. Cheng YM, Hull CM, Niven CM, Qi J, Allard CR, Claydon TW. Functional interactions of voltage sensor charges with an S2 hydrophobic plug in hERG channels. *J Gen Physiol.* 2013;142(3):289–303.
55. Subbiah RN, Kondo M, Campbell TJ, Vandenberg JJ. Tryptophan scanning mutagenesis of the HERG K⁺ channel: the S4 domain is loosely packed and likely to be lipid exposed. *J Physiol.* 2005;569(Pt 2):367–79.
56. Zhang M, Liu J, Jiang M, Wu DM, Sonawane K, Guy HR, Tseng GN. Interactions between charged residues in the transmembrane segments

- of the voltage-sensing domain in the hERG channel. *J Membr Biol.* 2005;207(3):169–81.
57. Guo J, Cheng YM, Lees-Miller JP, Perissinotti LL, Claydon TW, Hull CM, Thouta S, Roach DE, Durdagi S, Noskov SY, Duff HJ. NS1643 interacts around L529 of hERG to alter voltage sensor movement on the path to activation. *Biophys J.* 2015;108(6):1400–13.
 58. Gardner A, Wu W, Thomson S, Zangerl-Plessl EM, Stary-Weinzinger A, Sanguinetti MC. Molecular Basis of Altered hERG1 Channel Gating Induced by Ginsenoside Rg3. *Mol Pharmacol.* 2017;92(4):437–50.
 59. Panaghie G, Abbott GW. The role of S4 charges in voltage-dependent and voltage-independent KCNQ1 potassium channel complexes. *J Gen Physiol.* 2007;129(2):121–33.
 60. Posson DJ, McCoy JG, Nimigean CM. The voltage-dependent gate in MthK potassium channels is located at the selectivity filter. *Nat Struct Mol Biol.* 2013;20(2):159–66.
 61. Kapplinger JD, Tester DJ, Salisbury BA, Carr JL, Harris-Kerr C, Pollevick GD, Wilde AA, Ackerman MJ. Spectrum and prevalence of mutations from the first 2,500 consecutive unrelated patients referred for the FAMILION long QT syndrome genetic test. *Heart Rhythm.* 2009;6(9):1297–303.
 62. Anderson CL, Kuzmicki CE, Childs RR, Hintz CJ, Delisle BP, January CT. Large-scale mutational analysis of Kv11.1 reveals molecular insights into type 2 long QT syndrome. *Nat Commun.* 2014;5:5535.
 63. Ficker E, Obejero-Paz CA, Zhao S, Brown AM. The binding site for channel blockers that rescue misprocessed human long QT syndrome type 2 ether-a-go-go-related gene (HERG) mutations. *J Biol Chem.* 2002;277(7):4989–98.
 64. Li P, Chen X, Zhang Q, Zheng Y, Jiang H, Yang H, Gao Z. The human ether-a-go-go-related gene activator NS1643 enhances epilepsy-associated KCNQ channels. *J Pharmacol Exp Ther.* 2014;351(3):596–604.
 65. Lewis CA. Ion-concentration dependence of the reversal potential and the single channel conductance of ion channels at the frog neuromuscular junction. *J Physiol.* 1979;286:417–45.

Publisher's Note

Springer Nature remains neutral with regard to jurisdictional claims in published maps and institutional affiliations.